

**Half-skyrmion spin textures in polariton microcavities**P. Cilibrizzi,<sup>1,\*</sup> H. Sigurdsson,<sup>2,3</sup> T. C. H. Liew,<sup>2</sup> H. Ohadi,<sup>1</sup> A. Askitopoulos,<sup>1</sup> S. Brodbeck,<sup>4</sup> C. Schneider,<sup>4</sup> I. A. Shelykh,<sup>2,3</sup> S. Höfling,<sup>4,5</sup> J. Ruostekoski,<sup>6</sup> and P. Lagoudakis<sup>1</sup><sup>1</sup>*School of Physics and Astronomy, University of Southampton, Southampton, SO17 1BJ, United Kingdom*<sup>2</sup>*Division of Physics and Applied Physics, School of Physical and Mathematical Sciences, Nanyang Technological University 637371, Singapore*<sup>3</sup>*Science Institute, University of Iceland, Dunhagi-3, IS-107 Reykjavik, Iceland*<sup>4</sup>*Technische Physik, Wilhelm-Conrad-Röntgen-Research Center for Complex Material Systems, Universität Würzburg, Am Hubland, D-97074 Würzburg, Germany*<sup>5</sup>*SUPA, School of Physics and Astronomy, University of St Andrews, St Andrews, KY16 9SS, United Kingdom*<sup>6</sup>*Mathematical Sciences, University of Southampton, Southampton SO17 1BJ, United Kingdom*

(Received 20 January 2016; revised manuscript received 2 June 2016; published 25 July 2016)

We study the polarization dynamics of a spatially expanding polariton condensate under nonresonant linearly polarized optical excitation. The spatially and temporally resolved polariton emission reveals the formation of nontrivial spin textures in the form of a quadruplet polarization pattern both in the linear and circular Stokes parameters, and an octuplet in the diagonal Stokes parameter. The continuous rotation of the polariton pseudospin vector through the condensate due to TE-TM splitting exhibits an ordered pattern of half-skyrmions associated with a half-integer topological number. A theoretical model based on a driven-dissipative Gross-Pitaevskii equation coupled with an exciton reservoir describes the dynamics of the nontrivial spin textures through the optical spin-Hall effect.

DOI: [10.1103/PhysRevB.94.045315](https://doi.org/10.1103/PhysRevB.94.045315)**I. INTRODUCTION**

Skyrmions are *nonsingular* but topologically *nontrivial* spin textures [1], identified by a winding number, known as the *skyrmion number*, which corresponds to the number of times the spin vector continuously rotates across a finite region of space [2]. In particular, they are *nonsingular* because their spin is always defined in each point of space (i.e., there are no singularities) and *nontrivial* because they cannot be continuously transformed in a topologically trivial state (such as a ferromagnetic one, with all spins aligned in the same direction) and are hence relatively stable against perturbations [3]. This property makes skyrmions particularly attractive in the development of novel spintronics devices [3]. Although they were originally proposed by Skyrme in the field of nuclear physics [4], skyrmions have recently received special attention in solid state systems, such as semiconductor quantum wells [5] and ultrathin magnetic films [6,7], due to their potential in future applications, such as low-power ultradense magnetic memories and logic devices [7,8]. On a more fundamental level, three-dimensional (3D) skyrmions represent topological particlelike solitons in field theory, high-energy physics [9], and in atomic superfluids [10–13]. Moreover, two-dimensional (2D) skyrmions play a key role in the rotational properties of superfluid liquid <sup>3</sup>He [14,15] and in atomic spinor Bose-Einstein condensates [16–20], where they represent the vectorial counterpart of the quantized vortices of scalar superfluids and are usually referred to as coreless vortices, due to the absence of a vortex line singularity. Recently, skyrmion spin textures were theoretically predicted also in indirect excitons [21] and exciton-polariton condensates [22].

In this article, we report the formation and time evolution of 2D half-skyrmion spin textures in planar semiconductor

microcavities, which are suitable systems for studying the fundamental properties of dissipative bosonic systems, such as exciton-polariton condensates [23]. Exciton-polaritons, or hereafter polaritons, are composite bosonic quasiparticles formed by the strong coupling between heavy hole excitons, confined in quantum wells, and the photonic mode of a planar semiconductor microcavity [24]. By increasing the polariton population above a threshold density, polaritons can macroscopically occupy the ground state of the dispersion and form a nonequilibrium BEC [25], characterized by an inversionless amplification of the polariton emission [26,27] and macroscopic coherence over hundreds of microns [28]. Moreover, being bosons, polaritons possess an integer spin with two possible projections of the angular momentum ( $S_z = \pm 1$ ) on the structural growth axis ( $z$ ) of the microcavity, which correspond to the right and left circular polarization of the emitted photons. Superpositions of the  $S_z = \pm 1$  states give rise to the linear or elliptical polarization states of polaritons. An important effect, which capitalizes on the spin of polaritons, is the optical spin Hall effect (OSHE). After its first theoretical prediction [29], the OSHE has been observed in both strongly coupled [30] and weakly coupled [31] microcavities. The effect is a consequence of the energy splitting between transverse-electric (TE) and transverse-magnetic (TM) polarized modes [32], which occurs naturally in microcavities and represents an effective spin-orbit coupling. The initial demonstration of the optical spin Hall effect relied on resonant Rayleigh scattering [33], while spin currents were similarly generated using tightly focused laser spots in both resonant [30,31] and nonresonant configurations [34,35]. The TE-TM splitting also leads to the generation of vortices via spin-to-orbital angular momentum conversion [36,37], which was recently shown to be enhanced in tunable open microcavity structures [38].

In polariton microcavities, skyrmions were theoretically predicted under resonant excitation [22]. Differently from

\*Correspondence address: [pasquale.cilibrizzi@soton.ac.uk](mailto:pasquale.cilibrizzi@soton.ac.uk)

Ref. [22], we use a nonresonant excitation scheme to ensure that the original coherence of the laser is lost in the relaxation process [25]. We create a polariton condensate with a pseudospin orientation defined by the polarization of the excitation beam [39,40]. As the condensate expands, polaritons propagate over macroscopic distances, whilst their pseudospin collectively precesses. The three pseudospin orientations correspond to the three Stokes parameters [Eq. (1)] measured from analyzing the polarization of the emission. We record the formation of intricate spin textures in the spatial expansion of the polariton condensate. A quadruplet pattern is observed in the linear and circular Stokes parameters, while an octuplet is observed in the diagonal Stokes parameter. The formation of the observed spin textures is described in the framework of the driven-dissipative Gross-Pitaevskii equation through the optical spin Hall effect [29]. The half-skyrmion spin textures are unequivocally identified through the calculation of their topological charge, i.e. the skyrmion number [defined by Eq. (5)].

The article is organized as follows. In Sec. II we describe the experimental setup and the sample. In Sec. III the theoretical model is presented. In Sec. IV we report the main experimental results (IV A), discuss the skyrmion number (IV B), and describe the physical mechanism behind the formation of the half-skyrmion spin textures (IV C). Conclusions and perspectives are reported in Sec. V.

## II. SAMPLE AND EXPERIMENT

In this study we use a  $\lambda/2$  AlGaAs/AlAs microcavity sample [41] composed of 23 (27) pairs of AlGaAs/AlAs layers, forming the top (bottom) distributed Bragg reflectors (DBRs) and four triplets of 7 nm thick GaAs quantum wells (QWs) placed at the antinodes of the cavity electric field. The measured quality factor exceeds 9000 corresponding to a cavity photon lifetime of  $\sim 3.8$  ps. Strong coupling is obtained with a Rabi splitting energy of 14.5 meV. The microcavity wedge allows one to choose the detuning between the exciton and the cavity mode. All the data presented here are recorded at a negative detuning of  $-4.4$  meV. The sample is held in a cold-finger cryostat at a temperature of  $T \approx 6$  K.

To conduct the experiments we use the experimental setup schematically shown in Fig. S1 of the Supplemental Material (SM) [42]. We use a mode-locked Ti-sapphire pulsed laser to excite the sample at 1.687 eV, corresponding to the first reflectivity minimum above the stopband of the DBR. The pulse width of the laser is  $\sim 180$  fs, at a repetition rate of 80 MHz. The excitation beam is horizontally polarized and focused to an  $\sim 2 \mu\text{m}$  at FWHM spot diameter using a 0.4 numerical aperture (NA) microscope objective. The average fluence of the excitation beam is kept at  $\sim 600 \mu\text{J}/\text{cm}^2$  throughout these measurements. Photoluminescence (PL) is collected in reflection geometry through the excitation microscope objective, analyzed by a polarimeter composed of a  $\lambda/2$  or  $\lambda/4$  plate and a linear polarizer and projected on the entrance slit of a streak camera with 2 ps temporal resolution.

The spin of polaritons can be described in terms of the pseudospin ( $\mathbf{S}$ ) formalism, in which the polarization of the light emitted from the cavity is characterized by the linear ( $S_x$ ), diagonal ( $S_y$ ), and circular ( $S_z$ ) Stokes parameters, which

corresponds to the following degree of polarizations:

$$S_x = \frac{I_H - I_V}{I_H + I_V}, \quad S_y = \frac{I_D - I_A}{I_D + I_A}, \quad S_z = \frac{I_{\sigma_+} - I_{\sigma_-}}{I_{\sigma_+} + I_{\sigma_-}}, \quad (1)$$

where  $I_{H,D,\sigma_+}$  and  $I_{V,A,\sigma_-}$  are the measured intensities for the linear (horizontal, vertical, diagonal, antidiagonal) and circular ( $\sigma_+, \sigma_-$ ) components. Thus, by measuring the polarization of the emitted light, we record the polariton pseudospin state.

The spatial polarization dynamics of the polariton expansion was time-resolved using a tomography scanning technique. In this technique, the polarization analyzed PL intensity  $I(x, y, t)$  is projected at the entrance slit of the streak camera. By using a motorized mirror, we scan the vertical direction,  $y$ , of the PL image and acquire  $I(x, t)$  at different values of  $y$ . In this way, a 2D real space image  $I(x, y, t)$  can be reconstructed as a function of time.

## III. THEORETICAL MODEL

To model the spin dynamics of the polaritons BEC, we use a driven-dissipative Gross-Pitaevskii equation (2), describing the polariton field ( $\Psi_{\pm}$ ), which is then coupled to an excitonic rate equation (3) describing a hot exciton reservoir ( $\mathcal{N}_{\pm}$ ) generated by the nonresonant pump [43]:

$$i\hbar \frac{d\Psi_{\pm}}{dt} = \left[ \hat{E} - \frac{i\hbar}{2\tau_p} + \alpha |\Psi_{\pm}|^2 + \text{GP}_{\pm}(\mathbf{r}, t) + \left( g_R + \frac{i\hbar r_c}{2} \right) \mathcal{N}_{\pm} \right] \Psi_{\pm} + \hat{H}_{\text{LT}} \Psi_{\mp}, \quad (2)$$

$$\frac{d\mathcal{N}_{\pm}}{dt} = - \left( \frac{1}{\tau_x} + r_c |\Psi_{\pm}|^2 \right) \mathcal{N}_{\pm} + P_{\pm}(\mathbf{r}, t). \quad (3)$$

Here the indices represent the spin up/down ( $\pm$ ) basis. The coupled equations take into account a condensation rate ( $r_c$ ), corresponding to the rate at which excitons condense into polaritons and the energy blueshift of the polariton condensate due to interactions with excitons (with interaction strength  $g_R$ ). The condensed polariton field obeys approximately a parabolic dispersion  $\hat{E} = -\hbar^2 \nabla^2 / 2m^*$ , where  $m^*$  is the effective polariton mass. The polariton and exciton lifetimes are written  $\tau_p$  and  $\tau_x$ , respectively. Same-spin polariton interaction strength is characterized by the parameter  $\alpha$ . We neglect interactions between polaritons with opposite spins, which are typically small in magnitude [44] at energies far from the biexciton resonance [45]. The exciton reservoir is driven by a Gaussian pump,  $P_{\pm}(\mathbf{r}, t)$ , as described in Sec. II. For example, a horizontally polarized pump would correspond to  $\{P_+ = P_- : P_+, P_- \in \mathbb{R}^+\}$ . The interaction constant  $G$  represents an additional pump-induced shift which takes into account other excitonic contribution to the blueshift [43].

$\hat{H}_{\text{LT}}$  is the TE-TM splitting which mixes the spins of the polaritons:

$$\hat{H}_{\text{LT}} = \frac{\Delta_{\text{LT}}}{k_{\text{LT}}^2} \left( i \frac{\partial}{\partial x} \pm \frac{\partial}{\partial y} \right)^2, \quad (4)$$

with  $\Delta_{\text{LT}}$  being half the TE-TM splitting at wave vector  $k_{\text{LT}}$ . The strength of the TE-TM splitting is defined by the ratio  $\Delta_{\text{LT}}/k_{\text{LT}}^2$ , while the in-plane wave vector of polaritons

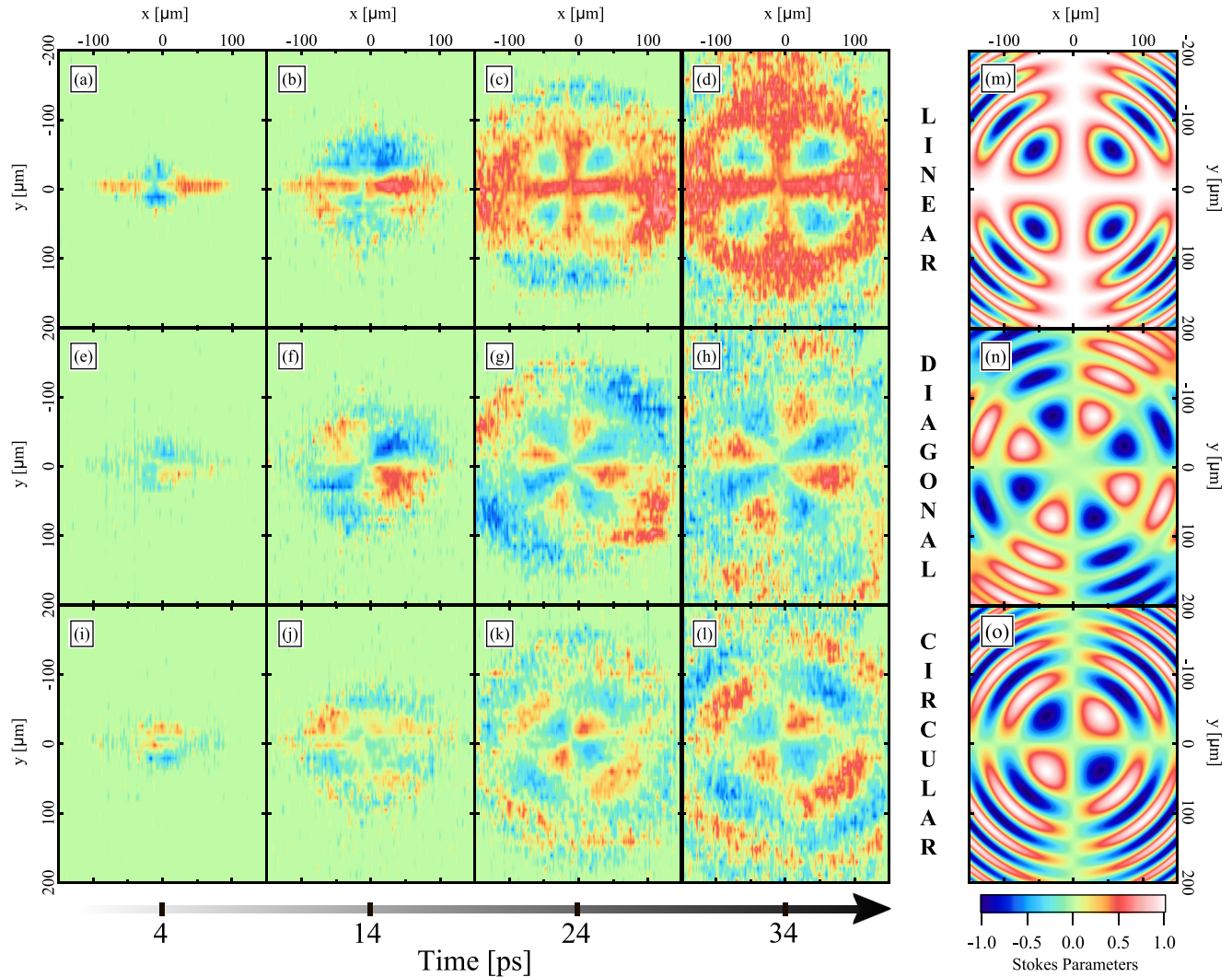


FIG. 1. Experimental real space linear (a)–(d), diagonal (e)–(h), and circular (i)–(l) Stokes parameters showing the formation dynamics of the polariton spin textures after pulsed optical excitation at 1.687 eV. The excitation beam is horizontally polarized. The zero time is defined at the PL onset as indicated in the spatial integrated intensity profiles in Figs. 4(a)–4(c). Theoretical real space linear (m), diagonal (n), and circular (o) Stokes parameters 34 ps after excitation with  $P_+/P_- = 1$  and  $P_+, P_- > 0$ . The color scale is the same for both the experimental and simulated results.

is given by the operator in the round brackets. In all the theoretical calculations the following parameters were set to  $\alpha = 2.4 \mu\text{eV} \mu\text{m}^2$ ,  $g_R = 1.5\alpha$ ,  $G = 4\alpha$ ,  $r_c = 0.01 \mu\text{m}^2 \text{ps}^{-1}$ ,  $\Delta_{\text{LT}}/k_{\text{LT}}^2 = 11.9 \mu\text{eV} \mu\text{m}^2$ ,  $\tau_p = 3.8 \text{ ps}$ , and  $\tau_x = 10 \text{ ps}$ .

## IV. DISCUSSION

### A. Experimental results

We investigate the formation mechanism of the spin textures under linearly polarized pulsed excitation. The nonresonant excitation creates electron-hole pairs in the QWs, which rapidly relax in energy toward the high  $k$  states of the exciton dispersion, giving rise to the exciton reservoir [46]. The lower polariton dispersion is populated through exciton-phonon and exciton-exciton scattering [24].

Here, we are interested in studying the pseudospin properties of polaritons which are directly related to the polarization of the emitted light by means of the Stokes vector [24]. By

performing polarization resolved measurements and using the tomography technique described in Sec. II, we time resolve the polariton emission and observe their spin dynamics in real space. A summary of the experimental data taken for the specific excitation energy of 1.687 eV and wave vector  $k \leq 2.9 \mu\text{m}^{-1}$  is shown in Fig. 1. The linear [Figs. 1(a)–1(d)], diagonal [Figs. 1(e)–1(h)], and circular [Figs. 1(i)–1(l)] components of the Stokes vector, calculated by applying Eq. (1), are shown at times 4 ps, 14 ps, 24 ps, and 34 ps upon relaxation. The theoretical simulations realized with the model and the parameters described in Sec. III are shown in Figs. 1(m)–1(o).

Under nonresonant excitation, the blueshift of polaritons is mainly determined by the interaction with the exciton reservoir [46,47]. In a recent work, we have shown how the exciton-exciton interactions in the proximity of the excitation spot directly affect the spin dynamics of polaritons, giving rise to a rotation of the circularly polarized spin textures, i.e.,

polariton spin whirls [48]. The whirling of the spin textures is a consequence of a spin imbalanced exciton reservoir, which results in a splitting  $g_R(\mathcal{N}_+ - \mathcal{N}_-)$  of polaritons acting as an effective magnetic field along the  $z$  direction [48]. In the current work, we use a lower excitation density compared to the spin whirls case [48] and explore the regime where the exciton density and consequently the splitting of the exciton reservoir  $g_R(\mathcal{N}_+ - \mathcal{N}_-)$  is not strong enough to cause any significant dynamic rotation in the polarization of the polariton condensate.

### B. Skyrmion number

The spin texture of a skyrmion is characterized by a winding number, known as the skyrmion number  $N_{sk}$ , which is defined by the surface integral

$$N_{sk} = \frac{1}{4\pi} \int \mathbf{S} \cdot \left( \frac{\partial \mathbf{S}}{\partial x} \times \frac{\partial \mathbf{S}}{\partial y} \right) dx dy. \quad (5)$$

Physically, it counts how many times  $\mathbf{S}$  wraps around the unit sphere when the integral covers the vortex core [2]. This winding number is conserved and skyrmion is topologically nontrivial whenever the boundary condition of  $\mathbf{S}$  is fixed, e.g., by energetics [20].

In the case of polariton microcavities, this vector corresponds to the total pseudospin vector [see Eq. (1) of the SM [42] for the full analytical expression of  $\mathbf{S}$  in polar coordinates  $r$  and  $\theta$ ], and its magnitude represents the total degree of polarization. Thus, by plotting the total pseudospin vector  $\mathbf{S}$  in the microcavity  $x$ - $y$  plane, the topological structure of the polariton half-skyrmion textures can be visualized. This is shown in Fig. 2(a) for the first quadrant, color-coded with the three Stokes components  $S_x, S_y, S_z$ . The regions where the total pseudospin vector  $\mathbf{S}$  is perpendicular to the  $x$ - $y$  plane correspond to the two circular polarization domains, with  $\mathbf{S}$  pointing up for  $\sigma_+$  (red) and down for  $\sigma_-$  (blue) domains. In

these domains, indicated for reference by the dashed black lines in Fig. 2(b), the skyrmion number  $N_{sk}$  is equal to  $-0.5$ .

Spin textures with a half-integer  $|0.5|$  topological charge correspond to *half-skyrmion* (also known as Merons [18] or Mermin-Ho vortices [15]) spin textures. In a skyrmion with a topological charge  $N_{sk} = \pm 1$ , the  $\mathbf{S}$  vector performs a  $\pi$  rotation with respect to the  $x$ - $y$  plane, over the integration domain, e.g.,  $S_z$  rotates continuously from  $\pm 1$  to  $\mp 1$ . In a half-skyrmion, on the other hand, the half integer topological charge ( $N_{sk} = \pm 0.5$ ) means that the total pseudospin vector performs only a  $\pi/2$  rotation over the integration domain, e.g., the  $S_z$  component goes from  $\pm 1$  to zero (or vice versa) from the half-skyrmion core to its domain boundary. Consequently, the  $\mathbf{S}$  vector, initially pointing toward the north (south), lies in the  $x$ - $y$  plane at the boundary of the integration domain. The sign of the topological number  $N_{sk}$  is determined first, by the rotation of  $S_z$  from the half-skyrmion core towards the integration boundary. Secondly, it is determined by the rotation of the in-plane spin ( $S_x, S_y$ ) along a closed path containing the half-skyrmion core. In Fig. 2(a), for example,  $N_{sk}$  retains the value  $-0.5$  from lobe to lobe in the same quadrant since  $S_z$  and ( $S_x, S_y$ ) both switch rotations between the half-skyrmion domains. Indeed, as shown in Fig. S2 of the SM [42],  $N_{sk}$  only changes sign between the quadrants of the system, a consequence of the OSHE. An analytical derivation showing the half-integer nature of the half-skyrmions is given in the SM, Sec. S2 [42].

It is worth noting that differently from spinor atomic condensates, where the nonlinear interactions within the condensate are important for the stability of the spin textures [20], here the half-skyrmions appear in the expansion of the condensate where polariton-polariton interactions do not play a significant role. It is the spatial potential profile of the polariton condensate that determines the formation of half-skyrmions (see Sec. IV D) and fixes the asymptotic orientation of the spins outside their cores, thus ensuring their topological stability.

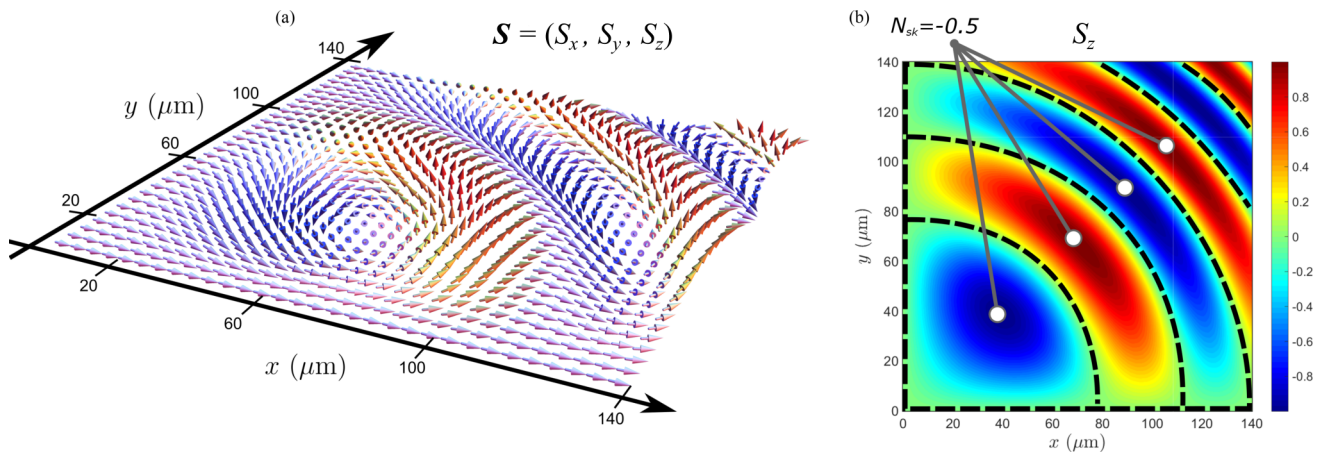


FIG. 2. (a) Vector field of the 2D polariton half-skyrmions, showing the rotation of the total pseudospin vector  $\mathbf{S} = (S_x, S_y, S_z)$  in the first quadrant of the microcavity  $x$ - $y$  plane [see Eq. (1) of the SM [42]]. The different colors of the vectors refer to the different polarization domains. In particular, red and blue refer to the  $\pm 1$  circular polarizations of  $S_z$ , respectively (with opposite orientations along the  $z$  axis), while pink in (a) and green in (b) to the linear and diagonal polarization components  $S_x, S_y$  (i.e., the pseudospin lying in the  $x$ - $y$  plane). (b) Circular Stokes components  $S_z$  showing the domains (circumscribed by the black dotted lines) where the skyrmion number  $N_{sk} = -0.5$  has been calculated using Eq. (5).

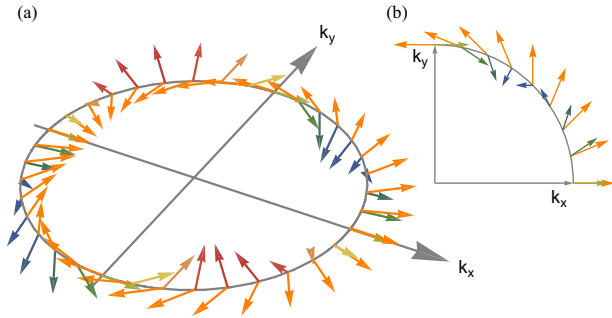


FIG. 3. (a) Sketch of the optical spin Hall effect in momentum space. The orange arrows show the effective magnetic field due to TE-TM splitting. The other arrows show the rotated polariton Stokes' vectors (starting from a linearly polarized state). The inset (b) shows the projections in the  $x$ - $y$  plane. Note that in any particular quadrant in reciprocal space, the sign of the  $y$  component of the Stokes' vector reverses sign. This behavior is at the origin of the eight-lobe textures observed in the diagonal Stokes pattern [see Figs. 1(g), 1(h), and Fig. 1(n)].

### C. Optical spin Hall effect

The polariton pseudospin dynamics is mainly determined by the TE-TM splitting of the photonic modes (LT splitting) [31,49]. At  $k > 0$ , polaritons are split into two nondegenerate modes with polarization along (L) and orthogonal (T) to  $\mathbf{k}$  and frequencies  $\omega_L(k)$  and  $\omega_T(k)$ , respectively, with the LT splitting  $\Delta_{LT}$ . This splitting acts as a wave-vector-dependent effective magnetic field ( $\mathbf{H}_{LT}$ ) in the plane of the microcavity ( $x$ - $y$  plane) making the pseudospin of polaritons precess (see SM [43], Sec. S3), similar to the Rashba field in the case of electron spin in doped QWs [50]. The effective magnetic field  $\Omega_{\mathbf{k}}$  lies in the plane of the microcavity and its components are [29]

$$\Omega_x = \frac{\Delta_{LT}}{\hbar k^2} (k_x^2 - k_y^2), \quad \Omega_y = \frac{\Delta_{LT}}{\hbar k^2} 2k_x k_y, \quad \Omega_z = 0. \quad (6)$$

Here,  $\mathbf{k} = (k_x, k_y)$  is the in-plane polariton wave vector.

The magnitude of the effective magnetic field is proportional to  $\Delta_{LT}$  and its direction in the plane of the microcavity depends on the direction of the polariton wave vector  $(k_x, k_y)$ . As shown in Fig. 3, different values of the wave vectors correspond to a different orientation of the effective magnetic field in  $k$  space (orange arrows), which in turn corresponds to a different precession of the pseudospin (colored arrows). In the case of GaAs microcavities this effective magnetic field is at the origin of the OSHE [29], which resembles the spin Hall effect in semiconductor thin layers [51]. In the spin Hall effect, however, initially unpolarized electrons spontaneously separate in spin up and spin down fractions due to the electron spin-orbit interactions, while in the OSHE the initial polarized polaritons rotate their pseudospin due to an effective magnetic field, analog of the spin-orbit interaction.

The OSHE, essentially consists in the angular polarized emission of the polaritons resulting in the appearance of alternating circularly or linearly polarized domains in the plane of the microcavity. The orientation of the spin polarized domains is determined by the polarization of the

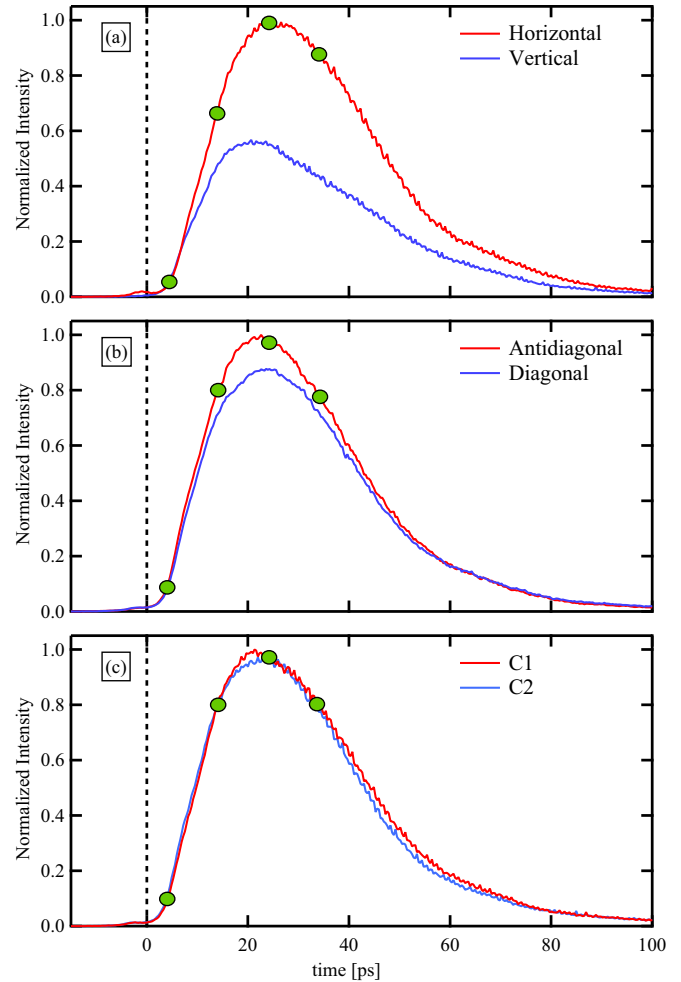


FIG. 4. Time-resolved, spatially integrated measurements of the (a) linear (b) diagonal, and (c) circular polarization components photoluminescence intensity, normalized and integrated over the area imaged in Figs. 1(a)–1(l), i.e.,  $(400 \times 300) \mu\text{m}^2$ . The zero time is defined at the PL onset, as shown in the graphs. The green circles correspond to the time of the snapshots shown in Figs. 1(a)–1(l).

pump. For example, in a previous work we have shown that under circularly polarized pump, the highly imbalanced spin population driven by the pump [39] results in concentric ring patterns of opposite circularly polarization [34]. Here, differently from Ref. [34], we excite our sample with a linearly polarized beam and observe skyrmionic textures theoretically predicted for atomic [11], indirect excitons [21] and polariton condensates [22] and the polarization beats experimentally observed in a microcavity under pulsed excitation [33]. In this case, the linearly polarized excitation results in linearly polarized condensates, as shown in Fig. 4. A small imbalance between the two circular polarization components still persists [Fig. 4(c)], as a consequence of the small ellipticity introduced by the high-NA excitation objective used in the experiment [48]. At high excitation densities this imbalance in the exciton reservoir,  $g_R(\mathcal{N}_+ - \mathcal{N}_-)$ , causes the rotation of the circularly polarized spin textures [48]. Here, due to the low excitation density regime the spin textures in the microcavity plane remains fixed in time (i.e., they do not rotate) [Figs. 1(i)–

1(i)], making the observed effect essentially linear (i.e., with negligible polariton-polariton interactions).

#### D. Formation dynamics of half-skyrmion spin textures

Polaritons are generated nonresonantly by means of a tight focused spot of  $\sim 2\ \mu\text{m}$  FWHM. Due to the interaction with the exciton reservoir, polaritons are radially expelled out of the excitation spot. As they propagate outside of the excitation spot, the potential energy is converted to kinetic energy, with wave vector determined by the gradient of the potential induced by the blueshift of the condensate. Depending on the wave vector, polaritons propagating in different directions experience different polarization rotation due to  $k$ -dependent precession of the polariton pseudospin around the effective magnetic field  $\mathbf{H}_{\text{LT}}$ . Consequently, the formation of the half-skyrmion spin textures in the plane of the microcavity is angle dependent (Fig. 1). In fact, for both linear [Figs. 1(a)–1(d)] and circular [Figs. 1(i)–1(l)] Stokes components, the polarization shows maxima in the diagonal direction, while it is almost suppressed in the vertical and horizontal direction, reproducing the polarization quadrature typical of the OSHE [29]. Specifically, the horizontal and vertical directions correspond to the position where the effective magnetic field is parallel or antiparallel to the pseudospin; thus no precession occurs [see, for example, Fig. 1(d)]. On the other hand, the diagonal directions (i.e., at  $45^\circ$  respect to the  $x$ - $y$  axis) correspond to the directions where the pseudospin precesses around a perpendicular oriented effective magnetic field, giving rise to spin textures that appear as domains of opposite polarization as polaritons propagate radially out of the excitation spot. Under CW excitation (see SM [42], Sec. S4) the generation of polaritons, sustained by the continuous injection of electron-hole pairs due to the nonresonant CW laser, allows us to observe the polariton spin precess twice with respect to its initial orientation. This corresponds to the appearance of external polarized lobes in real space [Figs. S4(a) and S4(b) of the SM [42]].

In addition to the linear and circular spin textures, here we show the diagonal Stokes component of the condensate, as shown in Figs. 1(e)–1(h). A characteristic eight-lobes texture centered around the excitation spot at  $(0,0)\ \mu\text{m}$  is observed [Figs. 1(g) and 1(h)]. The formation of this spin texture is due to the symmetry of the TE and TM states over the elastic circle in the  $(k_x, k_y)$  plane. In particular, the angle between the effective magnetic field ( $\mathbf{H}_{\text{LT}}$ ) and the polariton wave vector corresponds to a double angle ( $2\phi$ ) with respect to the  $x$  axis in the Poincaré sphere. As sketched in Fig. 3, at any particular quadrant in reciprocal space, the sign of the  $y$  component of the Stokes' vector reverses sign. Consequently, in each quadrant in  $k$  space (inset in Fig. 3) there will be two opposite

projections of the Stokes vector, which will correspond to the two opposite diagonal polarized lobes (for each quadrant) in real space [Figs. 1(g)–1(h)].

Theoretical simulations performed in the presence of disorder show that the half-skyrmion spin textures are stable against perturbations, such as structural defects naturally present in microcavities (see SM [42], Sec. S5).

#### V. CONCLUSIONS

In conclusion, we have studied the formation and time evolution of 2D half-skyrmion spin textures in a planar semiconductor microcavity. We have demonstrated theoretically and experimentally that the appearance of these nontrivial spin textures is due to the optical spin Hall effect, which originates from the TE-TM splitting of the propagating modes. We note that the major contribution to the observations reported here is due to the splitting of the cavity optical modes which, consequently, makes the effect essentially linear (i.e., with negligible polariton-polariton interactions). The calculation of the characteristic skyrmion number, associated with the topology of half-skyrmion spin textures, supports and completes the observation.

Vectorial textures with different topological charges have been studied in several physical systems, ranging from polarized optical beams [52], semiconductor lasers [53], and atomic spinor condensates [54]. The study of these topological objects helps to better clarify the link between different branches of physics and to gain an in depth understanding of other physical systems [55]. Compared to conventional condensed matter systems, polariton condensates in semiconductor microcavities provide a unique opportunity to study and characterize spinor dynamics since the condensate order parameter can be directly accessed through optical measurements in both real and momentum space. Moreover, depending on the polarization of the excitation pump, several spin textures can be realized (see, for example, Ref. [34]), making polariton microcavities a suitable system to envisage a deterministic control of the skyrmionic spin textures by external optical beams.

#### ACKNOWLEDGMENTS

P.C., S.H., and P.L. acknowledge support by the Engineering and Physical Sciences Research Council of UK through the ‘‘Hybrid Polaritonics’’ Program Grant (Project EP/M025330/1). H.S. and I.A.S. acknowledge the support from Rannis projects BOFEHYSS and Singaporean Ministry of Education under AcRF Tier 2 grant MOE2015-T2-1-055. I.A.S. thanks 5-100 program of Russian Federal Government.

All data supporting this study are openly available from the University of Southampton repository, see Ref. [56].

- 
- [1] M. Lewenstein, A. Sanpera, and V. Ahufinger, *Ultracold Atoms in Optical Lattices: Simulating Quantum Many-body Systems* (Oxford University Press, Oxford, 2012).  
 [2] N. Nagaosa and Y. Tokura, *Nat. Nanotechnol.* **8**, 899 (2013).

- [3] R. Ritz, *Nat. Nanotechnol.* **10**, 573 (2015).  
 [4] T. H. R. Skyrme, *Proc. R. Soc. A: Math., Phys. Eng. Sci.* **260**, 127 (1961).  
 [5] B. A. Bernevig, T. L. Hughes, and S.-C. Zhang, *Science* **314**, 1757 (2006).

- [6] X. Z. Yu, Y. Onose, N. Kanazawa, J. H. Park, J. H. Han, Y. Matsui, N. Nagaosa, and Y. Tokura, *Nature (London)* **465**, 901 (2010).
- [7] N. Romming, A. Kubetzka, C. Hanneken, K. von Bergmann, and R. Wiesendanger, *Phys. Rev. Lett.* **114**, 177203 (2015).
- [8] A. Fert, V. Cros, and J. Sampaio, *Nat. Nanotechnol.* **8**, 152 (2013).
- [9] N. Manton and P. Sutcliffe, *Topological Solitons* (Cambridge University Press, Cambridge, UK, 2004).
- [10] J. Ruostekoski and J. R. Anglin, *Phys. Rev. Lett.* **86**, 3934 (2001).
- [11] U. Al Khawaja and H. Stoof, *Nature (London)* **411**, 918 (2001).
- [12] R. A. Battye, N. R. Cooper, and P. M. Sutcliffe, *Phys. Rev. Lett.* **88**, 080401 (2002).
- [13] C. M. Savage and J. Ruostekoski, *Phys. Rev. Lett.* **91**, 010403 (2003).
- [14] P. W. Anderson and G. Toulouse, *Phys. Rev. Lett.* **38**, 508 (1977).
- [15] N. D. Mermin and T.-L. Ho, *Phys. Rev. Lett.* **36**, 594 (1976).
- [16] T. Mizushima, K. Machida, and T. Kita, *Phys. Rev. Lett.* **89**, 030401 (2002).
- [17] A. E. Leanhardt, Y. Shin, D. Kielpinski, D. E. Pritchard, and W. Ketterle, *Phys. Rev. Lett.* **90**, 140403 (2003).
- [18] L. S. Leslie, A. Hansen, K. C. Wright, B. M. Deutsch, and N. P. Bigelow, *Phys. Rev. Lett.* **103**, 250401 (2009).
- [19] J.-y. Choi, W. J. Kwon, and Y.-i. Shin, *Phys. Rev. Lett.* **108**, 035301 (2012).
- [20] J. Lovegrove, M. O. Borgh, and J. Ruostekoski, *Phys. Rev. Lett.* **112**, 075301 (2014).
- [21] D. V. Vishnevsky, H. Flayac, A. V. Nalotov, D. D. Solnyshkov, N. A. Gippius, and G. Malpuech, *Phys. Rev. Lett.* **110**, 246404 (2013).
- [22] H. Flayac, D. D. Solnyshkov, I. A. Shelykh, and G. Malpuech, *Phys. Rev. Lett.* **110**, 016404 (2013).
- [23] I. Carusotto and C. Ciuti, *Rev. Mod. Phys.* **85**, 299 (2013).
- [24] A. Kavokin, J. J. Baumberg, G. Malpuech, and F. P. Laussy, *Microcavities* (Oxford University Press, Oxford, 2007).
- [25] T. Byrnes, N. Y. Kim, and Y. Yamamoto, *Nat. Phys.* **10**, 803 (2014).
- [26] A. Imamoglu, R. J. Ram, S. Pau, and Y. Yamamoto, *Phys. Rev. A* **53**, 4250 (1996).
- [27] H. Deng, G. Weihs, D. Snoke, J. Bloch, and Y. Yamamoto, *Proc. Natl. Acad. Sci. U.S.A.* **100**, 15318 (2003).
- [28] B. Nelsen, G. Liu, M. Steger, D. W. Snoke, R. Balili, K. West, and L. Pfeiffer, *Phys. Rev. X* **3**, 041015 (2013).
- [29] A. Kavokin, G. Malpuech, and M. Glazov, *Phys. Rev. Lett.* **95**, 136601 (2005).
- [30] C. Leyder, M. Romanelli, J. P. Karr, E. Giacobino, T. C. H. Liew, M. M. Glazov, A. V. Kavokin, G. Malpuech, and A. Bramati, *Nat. Phys.* **3**, 628 (2007).
- [31] M. Maragkou, C. E. Richards, T. Ostatnický, A. J. D. Grundy, J. Zajac, M. Hugues, W. Langbein, and P. G. Lagoudakis, *Opt. Lett.* **36**, 1095 (2011).
- [32] G. Panzarini, L. C. Andreani, A. Armitage, D. Baxter, M. S. Skolnick, V. N. Astratov, J. S. Roberts, A. V. Kavokin, M. R. Vladimirova, and M. A. Kaliteevski, *Phys. Rev. B* **59**, 5082 (1999).
- [33] W. Langbein, I. Shelykh, D. Solnyshkov, G. Malpuech, Y. Rubo, and A. Kavokin, *Phys. Rev. B* **75**, 075323 (2007).
- [34] E. Kammann, T. C. H. Liew, H. Ohadi, P. Cilibrizzi, P. Tsotsis, Z. Hatzopoulos, P. G. Savvidis, A. V. Kavokin, and P. G. Lagoudakis, *Phys. Rev. Lett.* **109**, 036404 (2012).
- [35] C. Antón, S. Morina, T. Gao, P. S. Eldridge, T. C. H. Liew, M. D. Martín, Z. Hatzopoulos, P. G. Savvidis, I. A. Shelykh, and L. Viña, *Phys. Rev. B* **91**, 075305 (2015).
- [36] T. C. H. Liew, A. V. Kavokin, and I. A. Shelykh, *Phys. Rev. B* **75**, 241301 (2007).
- [37] F. Manni, K. G. Lagoudakis, T. K. Paraíso, R. Cerna, Y. Léger, T. C. H. Liew, I. A. Shelykh, A. V. Kavokin, F. Morier-Genoud, and B. Deveaud-Plédran, *Phys. Rev. B* **83**, 241307(R) (2011).
- [38] S. Dufferwiel, F. Li, E. Cancellieri, L. Giriunas, A. A. P. Trichet, D. M. Whittaker, P. M. Walker, F. Frasn, E. Clarke, J. M. Smith, M. S. Skolnick, and D. N. Krizhanovskii, *Phys. Rev. Lett.* **115**, 246401 (2015).
- [39] H. Ohadi, E. Kammann, T. C. H. Liew, K. G. Lagoudakis, A. V. Kavokin, and P. G. Lagoudakis, *Phys. Rev. Lett.* **109**, 016404 (2012).
- [40] G. Li, T. C. H. Liew, O. A. Egorov, and E. A. Ostrovskaya, *Phys. Rev. B* **92**, 064304 (2015).
- [41] J. Fischer, I. G. Savenko, M. D. Fraser, S. Holzinger, S. Brodbeck, M. Kamp, I. A. Shelykh, C. Schneider, and S. Höfling, *Phys. Rev. Lett.* **113**, 203902 (2014).
- [42] See Supplemental Material at <http://link.aps.org/supplemental/10.1103/PhysRevB.94.045315> for the description and the schematic of the experimental setup (Sec. S1), the half-skyrmion textures calculated in all the quadrants of the x-y plane together with the full analytical expression of the pseudospin S in polar coordinates (Sec. S2), a detailed description of the optical spin Hall effect in semiconductor microcavities (Sec. S3), the experimental formation of half-skyrmion spin textures under CW excitation (Sec. S4), and the theoretical simulations showing the formation of half-skyrmions in the presence of disorder (Sec. S5).
- [43] M. Wouters and I. Carusotto, *Phys. Rev. Lett.* **99**, 140402 (2007).
- [44] M. Vladimirova, S. Cronenberger, D. Scalbert, K. V. Kavokin, A. Miard, A. Lemaitre, J. Bloch, D. Solnyshkov, G. Malpuech, and A. V. Kavokin, *Phys. Rev. B* **82**, 075301 (2010).
- [45] N. Takemura, S. Trebaol, M. Wouters, M. T. Portella-Oberli, and B. Deveaud, *Phys. Rev. B* **90**, 195307 (2014).
- [46] C. Piermarocchi, F. Tassone, V. Savona, A. Quattropani, and P. Schwendimann, *Phys. Rev. B* **55**, 1333 (1997).
- [47] M. Pieczarka, M. Syperek, L. Dusanowski, J. Misiewicz, F. Langer, A. Forchel, M. Kamp, C. Schneider, S. Höfling, A. Kavokin, and G. Sek, *Phys. Rev. Lett.* **115**, 186401 (2015).
- [48] P. Cilibrizzi, H. Sigurdsson, T. C. H. Liew, H. Ohadi, S. Wilkinson, A. Askitopoulos, I. A. Shelykh, and P. G. Lagoudakis, *Phys. Rev. B* **92**, 155308 (2015).
- [49] P. Cilibrizzi, H. Ohadi, T. Ostatnický, A. Askitopoulos, W. Langbein, and P. Lagoudakis, *Phys. Rev. Lett.* **113**, 103901 (2014).
- [50] J. Sinova, D. Culcer, Q. Niu, N. A. Sinitsyn, T. Jungwirth, and A. H. MacDonald, *Phys. Rev. Lett.* **92**, 126603 (2004).
- [51] M. I. Dyakonov and V. I. Perel, *Phys. Lett. A* **35**, 459 (1971).
- [52] M. R. Dennis, *Opt. Commun.* **213**, 201 (2002).
- [53] F. Prati, G. Tissoni, M. San Miguel, and N. B. Abraham, *Opt. Commun.* **143**, 133 (1997).
- [54] A. Hansen, J. T. Schultz, and N. P. Bigelow, *Optica* **3**, 355 (2016).
- [55] Editorial, *Nat. Photon.* **8**, 1 (2014).
- [56] <http://dx.doi.org/10.5258/SOTON/386411>.